DMD Fast Forward. Published on January 23, 2018 as DOI: 10.1124/dmd.117.079723
This article has not been copyedited and formatted. The final version may differ from this version.



# Metabolic profiling of the novel HIF2α inhibitor PT2385 *in vivo* and *in vitro*

Cen Xie, Xiaoxia Gao, Dongxue Sun, Youbo Zhang, Kristopher W. Krausz, Xuemei Qin, Frank J. Gonzalez

Laboratory of Metabolism, Center for Cancer Research, National Cancer Institute, National Institutes of Health, Bethesda, Maryland, USA (C.X., X.G., D.S., Y.Z., K.W.K., and F.J.G.); Modern Research Center for Traditional Chinese Medicine, Shanxi University, Taiyuan, Shanxi, P.R. China (X.G. and X.Q.).

**Running title:** Metabolic profiling of PT2385

**Corresponding authors:**

Frank J. Gonzalez, Laboratory of Metabolism, Center for Cancer Research, National Cancer Institute, National Institutes of Health, Bethesda, Maryland 20892, USA. E-mail: gonzalef@mail.nih.gov; and Xiaoxia Gao, Associate Professor, Modern Research Center for Traditional Chinese Medicine, Shanxi University, Taiyuan, Shanxi, 030006, China. Email: gaoxiaoxia@sxu.edu.cn

**Number of text pages:** 25

**Number of tables:** 1

**Number of figures:** 7

**Number of references:** 35

**Number of words:**

Abstract: 250

Introduction: 564

Discussion: 1046

**Abbreviations**

ARNT, aryl hydrocarbon receptor nuclear translocator; ccRCC, clear cell renal cell carcinoma; CYP, cytochrome P450; FMO, flavin mono-oxygenase; FXR, farnesoid X receptor; HIF-2α, hypoxia inducible factor-2α; HLM, human liver microsome; MDA, multivariate data analysis; MLM, mice liver microsome; NAC, *N*-acetylcysteine; NADPH, β-Nicotinamide adenine dinucleotide 2'-

phosphate reduced; OPLS-DA, orthogonal projections to latent structures discriminant analysis; PCA, principle components analysis; TCA, taurocholic acid; T-β-MCA, tauro-β-muricholic acid; UDPGA, uridine 5'-diphosphoglucuronic acid trisodium salt; UGT, UDP-glucuronosyltransferase; UPLC-HRMS, ultra-performance liquid chromatography-high resolution mass spectrometer; Q/TOF MS, quadrupole/time-of-flight mass spectrometer; VHL, von Hippel-Lindau

**Abstract**

PT2385 is a first-in-class, selective small molecule inhibitor of hypoxia inducible factor-2α (HIF-2α) developed for the treatment of advanced clear cell renal cell carcinoma. Preclinical results demonstrated that PT2385 has potent anti-tumor efficacy in mouse xenograft models of kidney cancer. It also has activity toward metabolic disease in a mouse model. However, no metabolism data is currently publically available. It is of great importance to characterize the metabolism of PT2385 and identify its effect on systemic homeostasis in mice. High-resolution mass spectrometry-based metabolomics was performed to profile the biotransformation of PT2385 and PT2385-induced changes in endogenous metabolites. Liver microsomes and recombinant drug-metabolizing enzymes were used to determine the mechanism of PT2385 metabolism. Real-time PCR analysis was employed to investigate the reason for the PT2385-induced bile acid dysregulation. A total of 12 metabolites of PT2385 were characterized, generated from hydroxylation (M1, M2), di-hydroxylation and desaturation (M3, M4), oxidative-defluorination (M7), glucuronidation (M8), *N*-acetylcysteine conjugation (M9), and secondary methylation (M5, M6) and glucuronidation (M10, M11, and M12). CYP2C19 was the major contributor to the formation of M1, M2 and M7, UGT2B17 to M8, and UGT1A1/3 to M10 – M12. The bile acid metabolites taurocholic acid and tauro-β-muricholic acid were elevated in serum and liver of mice after PT2385 treatment. Gene expression analysis further revealed that intestinal HIF-2α inhibition by PT2385 treatment upregulated the hepatic expression of CYP7A1, the rate-limiting enzyme in bile acid synthesis. This study provides metabolic data and an important reference basis for the safety evaluation and rational clinical application of PT2385.

DMD Fast Forward. Published on January 23, 2018 as DOI: 10.1124/dmd.117.079723
This article has not been copyedited and formatted. The final version may differ from this version.



## Introduction

It has been estimated that nearly 63,990 new cases of kidney cancer will be diagnosed and more than 14,400 people will die from this disease in 2017 (Siegel et al., 2017). Clear cell renal cell carcinoma (ccRCC) is the most common kidney cancer, representing 70 – 75% of all primary renal cell malignancies (Muglia and Prando, 2015). In more than 90% of ccRCC patients, von Hippel-Lindau (VHL) protein is defective leading to the activation of hypoxia-inducible factor-α (HIF-α) (Gnarra et al., 1994; Sato et al., 2013). The HIF-α family, consisting of HIF-1α, HIF-2α, and the less well characterized HIF-3α, is an oxygen-sensitive transcription factor family that regulates anaerobic metabolism, energy metabolism, angiogenesis, cell proliferation, differentiation and survival (Semenza and Wang, 1992; Keith et al., 2012). HIF-α levels are regulated by a ubiquitin-proteasome degradation pathway mediated by the E3 ubiquitin ligase VHL, and by the action of prolyl hydroxylase enzymes that hydroxylate the oxygen-sensing subunit of HIF-α leading to recognition by VHL and ultimate degradation (Maxwell et al., 1999; Epstein et al., 2001). Over the past decades, accumulating data reveal an oncogenic role for HIF-2α in VHL-defective ccRCC and highlight the therapeutic potential of HIF-2α antagonism in ccRCC treatment (Kondo et al., 2002; Gordan et al., 2007; Bertout et al., 2009; Vanharanta et al., 2013).

PT2385, [*S*]-3((2,2-difluoro-1-hydroxy-7-(methylsulfonyl)-2,3-dihydro-1H-inden-4-yl)oxy)-5-fluorobenzonitrile (Fig. 1), is a selective and potent small-molecule HIF-2α inhibitor identified by a structure-based design approach. It allosterically blocks the heterodimerization of HIF-2α with its partner aryl hydrocarbon receptor nuclear translocator (ARNT)/HIF-1β, while having no effect on HIF-1α (Wallace et al., 2016). Preclinical data revealed that PT2385 treatment suppresses gene expression essential for tumor growth, proliferation, and angiogenesis in ccRCC cell lines and in tumor xenografts. In ccRCC mouse models, PT2385 also inhibits tumor growth and displays better efficacy than sunitinib, a currently approved first-line anti-angiogenesis drug, without

cardiovascular adverse effects (Wallace et al., 2016). Similarly, the structural analogue PT2399 also causes tumor regression in mouse models of primary and metastatic pVHL-defective ccRCC and patient-derived xenografts (Chen et al., 2016; Cho et al., 2016). Phase I results demonstrated that PT2385 is well tolerated and showed promising efficacy in a highly pretreated patient population (Chen et al., 2016; Courtney et al., 2017). PT2385 is currently under evaluation in the phase II clinical trial for the treatment of ccRCC. The primary objective of this trial is to examine the overall response rate of VHL-associated ccRCC tumors in untreated patients. There is another phase II study of PT2385 for patients with recurrent glioblastoma. Besides antineoplastic activity, a recent report also showed that the inhibition of intestinal HIF-2α signaling by PT2385 substantially prevents and reverses obesity, insulin resistance and hepatic steatosis in mice (Xie et al., 2017).

To fully characterize the efficacy and safety of drug candidates, the metabolism must be determined during drug discovery and development (Xie et al., 2012). The profiling of endogenous metabolism is also helpful in understanding the action of drug on the organism. Metabolomics is a promising tool to determine the metabolic fate of a drug and alterations of endogenous substances that can serve as biomarkers for drug efficacy and toxicity (Fang and Gonzalez, 2014). Herein, ultra-performance liquid chromatography-high-resolution mass spectrometry (UPLC-HRMS)-based metabolomics was applied to elucidate PT2385 metabolism and interactions, including identification of metabolites, the major drug metabolizing enzymes involved, and its influence on bile acid homeostasis, through combining *in vitro* incubation studies and *in vivo* animal models.

DMD Fast Forward. Published on January 23, 2018 as DOI: 10.1124/dmd.117.079723
This article has not been copyedited and formatted. The final version may differ from this version.



## Materials and Methods

**Chemicals and reagents.** PT2385 was purchased from by MedChem Express (Monmouth Junction, NJ). β-Nicotinamide adenine dinucleotide 2'-phosphate reduced tetrasodium salt hydrate (NADPH), uridine diphosphate glucuronic acid (UDPGA), taurocholic acid (TCA), tauro-β-muricholic acid (T-β-MCA), and alamethicin were purchased from Sigma-Aldrich (St. Louis, MO). All other reagents were of the highest grade commercially available. Livers from untreated 6-week-old male C57BL/6N mice were used to prepare mouse liver microsomes (MLMs) as previously described (Meijer et al., 1987). Human liver microsomes (HLMs), recombinant cytochromes P450s (CYPs, 1A1, 1A2, 1B1, 2A6, 2B6, 2C8, 2C9, 2C19, 2D6, 2E1, 3A4, 3A5, and 4A11), flavin-containing monooxygenase (FMOs, FMO1, FMO3 and FMO5), and UDP-glucuronosyltransferase (UGTs, 1A1, 1A3, 1A4, 1A6, 1A9, 2B4, 2B7, 2B10, 2B15, and 2B17) were purchased from Corning Life Sciences (Tewksbury, MA, USA).

**Animals.** Male C57BL/6N mice were obtained from Charles River Laboratories (Wilmington, MA). Male *Hif2a*$^{fl/fl}$ (control) and *Hif2a*$^{\Delta IE}$ (intestine-specific *Hif2a* disruption) mice were generated and maintained as previously described (Xie et al., 2017). Mice were housed in a temperature- and humidity-controlled room and maintained under a standard 12 h light/12 h dark cycle with water and chow provided ad libitum. Mouse handling was performed in accordance with an animal study protocol approved by the National Cancer Institute Animal Care and Use Committee.

Seven male C57BL/6N (6- to 8-week-old) mice were divided into a control group ($n$ = 4) and PT2385-treated group ($n$ = 3). PT2385 suspended in 0.5% sodium carboxymethyl cellulose, 2.5% Tween 80 and 2.5% dimethyl sulfoxide was given by oral gavage at a dose of 50 mg/kg body weight, and control mice were treated with vehicle (0.5% sodium carboxymethyl cellulose, 2.5%

Tween 80 and 2.5% dimethyl sulfoxide). Urine and feces samples were collected for 24 h after administration. Blood samples were collected by retro-orbital bleeding at 3 and 24 h, respectively. After centrifugation for 10 min at 8,000×g, serum was obtained for metabolite analysis. Gallbladder, intestine mucosa and liver samples were collected after the mice were killed. Following centrifugation for 10 min at 15,000 × g, bile samples were collected. Liver samples were also collected from 12-week-old male littermate *Hif2a*$^{fl/fl}$ and *Hif2a*$^{\Delta IE}$ mice ($n$ = 5/group), respectively. All samples were stored at −80°C until analysis.

**Samples preparation.** For sample preparation, 30 μl of serum was deproteinizated with 60 μl of acetonitrile containing 2 μM chlorpropamide (internal standard, IS). After centrifugation for 10 min at 15,000 × g, 50 μl of the supernatant were diluted with 50 μl of water containing 0.1% formic acid. Urine samples were prepared by mixing 30 μl of urine with 60 μl of 66% aqueous acetonitrile containing 2 μM IS. The feces were pulverized and 1/20 (wt/v) 66% aqueous acetonitrile (2 μM IS) was added for extraction followed by centrifugation. An aliquot of 2 μl of bile sample was deproteinizated with 200 μl of acetonitrile containing 2 μM IS. After centrifugation for 10 min at 15,000 × g, the supernatants were diluted with 800 μl of water containing 0.1% formic acid. All samples were centrifuged at 15,000 × g for 10 min, and 5 μl aliquot of the supernatants was injected into a Waters UPLC-quadrupole/time-of-flight mass spectrometer (UPLC-Q/TOF MS) (Waters Corporation, Milford, MA).

***In vitro* incubation reaction to analyze the metabolic pathway of PT2385.** For liver microsomes, the incubation system (200 μL) contained 50 mM Tris–HCl buffer solution (pH 7.4), 0.5 mg/ml HLM or MLM, 5 mM $MgCl_2$, 2 mM freshly prepared UDPGA, 25 μg/ml alamethicin and 10 μM PT2385. The mixtures were pre-incubated at 37°C for 3 min and reactions initiated with 2 mM freshly prepared NADPH. The incubation mixtures without MLM (or HLM), NADPH,

DMD Fast Forward. Published on January 23, 2018 as DOI: 10.1124/dmd.117.079723
This article has not been copyedited and formatted. The final version may differ from this version.



UDPGA and PT2385 were used as the controls. The incubation system for recombinant human CYPs was similar to the liver microsomes incubation system, except that the microsomes were substituted with 50 nM recombinant enzymes and UDPGA was excluded. The incubation system for recombinant human UGTs contained 50 mM Tris–HCl buffer solution (pH 7.4), 50 nM CYP2C19, 5 mM $MgCl_2$, 2 mM UDPGA, 2 mM NADPH and 10 μM PT2385. The reactions were stopped by adding 200 μL ice-cold acetonitrile containing 2 μM IS after 60 min. After centrifugation at 15,000 × g for 10 min, a 5 μl aliquot of the supernatant was injected into a UPLC-Q/TOF MS. The relative abundance (peak area ratio of metabolite/IS) is given.

**UPLC-HRMS analysis.** Metabolite profiling and identification were performed on an Acquity UHPLC/Premier Q-TOF MS (Waters Corp, Milford, MA) with an electrospray ionization source. Separation was achieved on an Acquity $C_{18}$ BEH UPLC column (50 mm × 2.1 mm i.d., 1.7 μm; Waters Corp.). The mobile phase consisted of water containing 0.1% formic acid (A) and acetonitrile containing 0.1% formic acid (B). The gradient condition was used. The flow rate of the mobile phase was set at 0.4 ml/min. Column temperature was maintained at 40 °C throughout the run. Data were collected in the negative ion mode on a Q-TOF mass spectrometer, which was operated in a full-scan mode at *m/z* 50 – 850. Nitrogen was used as both cone gas (50 L/h) and desolvation gas (600 L/h). Source desolvation temperatures were set at 120 °C and 350 °C, respectively. The capillary voltage and cone voltage were 3000 and 20 V, respectively. The structures of metabolites were elucidated by tandem MS fragmentography with collision energies ranging from 15 to 40 eV.

**Data processing and multivariate data analysis (MDA).** Progenesis QI software (Waters Corp.) was used to deconvolute the chromatographic and mass spectrometric data. A multivariate data matrix containing information on sample identity, ion identity (Rt and m/z), and ion abundance was generated through centroiding, deisotoping, filtering, peak recognition, and integration. The

data matrix was further analyzed using SIMCA version 14.1 software (Umetrics, Kinnelon, NJ). Principle component analysis (PCA) was used to examine the separation of control group and PT2385-treated group. Orthogonal projections to latent structures discriminant analysis (OPLS-DA) was used to analyze the data to identify the major latent variables in the data matrix. Potential metabolites were identified by analyzing the ions contributing to the separation of sample groups in the loading scatter plots.

**Real-time PCR analysis.** Total RNA from frozen intestine mucosa and liver was extracted with TRIzol reagent (Invitrogen, Carlsbad, CA). cDNA was synthesized from 1 μg total RNA using qScript cDNA SuperMix (Gaithersburg, MD). Real-time PCR primer sequences are included in the Supplementary Table 1. The relative amount of each mRNA was calculated after normalizing to their corresponding *β-actin* mRNA, and the results expressed as fold change relative to the control group.

**Statistical analysis.** Experiment values were presented as mean ± s.e.m. Statistical analysis was performed using Prism version 7.0 (GraphPad Software, San Diego, CA). Statistical significance between two groups was determined using two-tailed Student's t-test. P values of less than 0.05 were considered to be significant. Power analysis were performed using StatMate version 2.0 (GraphPad Software).

DMD Fast Forward. Published on January 23, 2018 as DOI: 10.1124/dmd.117.079723
This article has not been copyedited and formatted. The final version may differ from this version.



## Results

**Metabolomics analysis to trace metabolites for exposure to PT2385.** The chromatographic and mass fragmentation pattern of the reference PT2385 was first investigated. PT2385 eluted at 6.0 min (Fig. 1A) with a deprotonated molecular ion at *m/z* 382.0365 in the negative mode; however, the most abundant peak was an in-source fragment ion at *m/z* 362.0325 due to the neutral loss of a hydrogen fluoride moiety (Fig. 1B). The MS/MS spectrum of PT2385 gave major fragment ions at *m/z* 347.0089, 342.0236, 282.0390, 263.0400, 235.0438, and 136.0203 (Fig. 1C), and the tentative fragmentation patterns were proposed in Fig. 1D. Typically, the fragment ion at *m/z* 342.0234 was formed via the double dehydrofluorinations and *m/z* 347.0089 ion was formed via the loss of methyl free radical beside the sulfonyl combined with dehydrofluorinationa. The fragment ion at *m/z* 136.0203 was characteristic of the fluorobenzonitrile moiety, acting as a diagnostic ion for metabolic elucidation on the fluorobenzonitrile ring.

UPLC-HRMS analysis coupled with MDA was used to profile the PT2385 metabolites found in mice. Unsupervised PCA separated the control and PT2385 treatment groups from feces, urine, bile, and serum samples (Fig. 2). The OPLS-DA loading S-plot showed the major ions contributing to the separation containing the parent compound (M0) and metabolites (M1 – M12). Detailed information on these metabolites are shown in Table 1.

**Metabolite elucidation in mice.** M1 and M2, detected in serum, feces, urine and bile, were eluted at 5.5 and 5.7 min, respectively. The deprotonated molecular ions at m/z 398.0313 were 16 Da higher than the parent compound, indicating hydroxylation. The presence of m/z 151.0067 fragment ion suggested that the oxygen was introduced in the fluorobenzonitrile moiety (Fig. 3A). M2 gave the major fragments at m/z 378.0247, 358.0194, 330.0266, and 251.0368 without a dehydration ion, implying the oxygen might be incorporated in the benzene ring bound with a methylsulfonyl group (Fig. 3B).

DMD Fast Forward. Published on January 23, 2018 as DOI: 10.1124/dmd.117.079723
This article has not been copyedited and formatted. The final version may differ from this version.



M3 and M4 were eluted at 5.3 and 5.4 min in feces, respectively. They possessed the deprotonated molecular ions at *m/z* 412.0156, which were 30 Da higher than PT2385, indicating dihydroxylation combined with desaturation. The possible oxidation site might be somewhere in both the benzene rings. The MS/MS fragments and the proposed fragmentation mechanism are shown in Fig. 3C.

M5 and M6 at *m/z* 426.0297 were detected at 5.8 and 5.9 min in the feces and urine, respectively. The elemental composition of them was supposed to be $C_{18}H_{12}F_3NO_6S$, indicating methylation of M3 and M4, which was supported by the observation of a typical fragment ion at *m/z* 411.0040 formed by neutral loss of methyl free radical in the MS/MS spectrum (Fig. 3D).

M7 was detected in the feces and bile, eluted at 5.6 min. The deprotonated molecular ion at *m/z* 380.0421, corresponding to the elemental composition of $C_{17}H_{13}F_2NO_5S$, was 2 Da lower than those of PT2385. Likewise, its fragment ions at *m/z* 360.0315, 340.0262, 233.0468, and 134.0253 were also 2 Da lower than the corresponding fragment ions of PT2385 (Fig. 3E). Analysis of the accurate mass showed that the loss of 2 Da was attributed to defluorination and the incorporation of a hydroxyl group. According to fluorine reactivity in a published report (Xie et al., 2013), this suggested that hydroxyl substitution of fluorine in the fluorobenzonitrile portion of the molecule.

M8 exhibited the deprotonated molecular ion at *m/z* 558.0701 at 5.5 min in urine, bile and serum, which was 176 Da higher than that of PT2385, indicative of glucuronidation. In liver microsomal incubations supplemented with UDPGA, M8 was the only metabolite formed, further supporting that M8 is a direct glucuronide conjugate of PT2385. The only possible position was at the aliphatic hydroxyl group. M9 showed the deprotonated molecular ion at *m/z* 543.0534 at 5.8 min in urine, which was 161 Da higher than that of PT2385, indicating a *N*-acetylcysteine (NAC) conjugate of PT2385. MS/MS fragmentation behavior confirmed that NAC was attached to the fluorobenzonitrile moiety (Fig. 3F). M10 and M11 were eluted at 4.8 and 5.1 min, respectively, in

urine and bile. Their deprotonated molecular ion (*m/z* 574.0661) was 176 Da higher than that of M1 and M2, suggesting that they were glucuronide conjugates of M1 and M2, respectively, most likely at the new phenolic hydroxyl group (Fig. 3G, 3H). M12 was detected in the bile and eluted at 5.0 min. The deprotonated molecular ion (*m/z* 557.0758) was 176 Da higher than that of M7, indicating that it was a glucuronide conjugate of M7 at the phenolic hydroxyl group. The proposed metabolic pathways of PT2385 in mice are depicted in Fig. 4.

***In Vitro* Biotransformation of PT2385 by liver microsomes.** To more fully determine the biotransformation mechanism of PT2385, the metabolism of PT2385 in HLM and MLM was studied. The phase I metabolites M1, M2, M3, M4, and M7 appeared in the NADPH-supplemented incubation systems, but was absent without adding NADPH (Fig. 5A, 5B), indicating that the formation of these oxidative metabolites was NADPH and CYP-dependent. In the presence of UDPGA, M8 was detected. The formation of glucuronide conjugates M10 – M12 were only observed in the incubation system with the presence of both UDPGA and NADPH, but were not detected in the system only with NADPH or UDPGA (Fig. 5A, 5B). This was consistent with the glucuronide conjugates (M10, M11 and M12) transformed from the oxidative metabolites (M1, M2 and M7), the formation of which required NADPH as a co-factor. HLM and MLM incubations yielded identical metabolic profiles toward PT2385, which demonstrated that mouse may be a suitable animal model to predict PT2385 metabolism and toxicity in humans.

**CYP2C19 is the predominant enzyme responsible for PT2385 oxidative metabolism.** Identification of the enzymes involved in the biotransformation pathways can facilitate a more complete understanding of an inter-individual response to PT2385. Therefore, the catalytic activities of a panel of human recombinant CYP and FMO enzymes towards oxidizing PT2385 were examined. CYP2C19 was identified as the principle isoform that mediated the oxidative metabolism of PT2385, while to a much lesser extent, CYP1A1, CYP1A2, CYP2C9, CYP2D6, and CYP3A4

DMD Fast Forward. Published on January 23, 2018 as DOI: 10.1124/dmd.117.079723
This article has not been copyedited and formatted. The final version may differ from this version.



also catalyzed M1 and M2 formation and CYP1A2 exhibited oxidative defluorination activity to form M7 (Fig. 5C, 5D, 5E).

**Multiple UGTs participates in PT2385 glucuronidation.** Because several glucuronide conjugates were derived from oxidative metabolites, CYP2C19 and NADPH was included in the recombinant UGT incubation systems. Among all the UGTs examined, UGT2B17, followed by UGT2B7, UGT2B15 and UGT1A6 were involved in the formation of M8 (Fig. 5F); UGT1A1, followed by UGT1A3, UGT1A9, UGT2B15, and UGT2B17 appeared to be responsible for the formation of M10 and M11 (Fig. 5G, 5H); and UGT1A1, UGT1A3, followed by UGT1A9, UGT2B4, UGT2B15, and UGT2B17 played a role in the formation of M12 (Fig. 5I). The generation of different glucuronide conjugates of PT2385 were catalyzed by different subsets of UGTs, implying the different conjugation sites and supporting that the structure elucidation was reasonable.

**Metabolomics analysis revealed unexpected PT2385-induced bile acid disruption.** To understand the *in vivo* effects of PT2385, metabolomics analysis was used to profile the endogenous metabolites in the 24-h serum and liver from PT2385-treated mice. MDA analysis was applied to analyze the data sets from both vehicle- and PT2385-treated groups. As expected, PCA modeling of mouse serum showed that samples from PT2385-treated mice clustered away from the controls, indicating notable metabolic changes between these two groups (Fig. 6A). The OPLS-DA loading S-plot showed that the major ions contributing to the separation displayed the deprotonated molecular ions at *m/z* 514.2842, and 514.2839 (Fig. 6B). Based on the metabolomics database (https://metlin.scripps.edu/landing_page.php?pgcontent=mainPage), these ions were assumed to be bile acids. The typical *m/z* with the chromatographic retentions and MS/MS spectra indicated that they were TCA and T-β-MCA, which were further confirmed by comparisons with authentic standards. Likewise, TCA and T-β-MCA were also the major ions contributing to the separation of

liver samples (Fig. 6C, 6D). Taken together, PT2385 treatment significantly elevated TCA and T-β-MCA levels in serum and liver (Fig. 6E, 6F).

**PT2385 upregulates bile acid synthesis-related gene expression.** To further determine the mechanism for PT2385-induced bile acid disruption, the gene expression of enzymes in bile acid synthesis was investigated. The results showed that treatment with PT2385 significantly upregulated the mRNA level of Cyp7a1 encoding CYP7A1, the rate-limiting enzyme in bile acid synthesis (Fig. 7A). Farnesoid X receptor (FXR) serves as a bile acid sensor and plays an important role in regulation of bile acid homeostasis in enterohepatic circulation (Matsubara et al., 2013). Both hepatic and intestinal FXR controls bile acid transport and synthesis (Li and Chiang, 2015), but PT2385 treatment did not alter either hepatic or intestinal FXR signaling (Fig. 7B, 7C). Furthermore, intestine-specific *Hif2a* ablation substantially upregulated Cyp7a1 mRNA in liver. These data suggested that PT2385 disrupted bile acid homeostasis through the inhibition of intestinal HIF-2α signaling.

**Discussion**

PT2385 is a selective and potent HIF-2α inhibitor and showed promising efficacy in the treatment of advanced ccRCC and metabolic disease (Wishart, 2016; Xie et al., 2017). PT2385 was rapidly absorbed with a median $t_{max}$ of 2 h and a mean $t_{1/2}$ of 17 h in ccRCC patients (Courtney et al., 2017). However, detailed metabolic information is currently publically unavailable. Therefore, in the present study, the metabolic pathways of PT2385 were elucidated with the combined use of *in vivo* and *in vitro* models.

PT2385 is extensively metabolized in mice, since the parent drug is only a minor component in urine and bile after oral administration to mice. The primary routes of PT2385 biotransformation involve hydroxylation, oxidative defluorination and glucuronidation. The hydroxylated metabolite M1 and glucuronide conjugate M8 are the major urinary metabolites and M8 is the major biliary metabolite. The parent drug is the most abundant drug-related material in feces, which could be largely attributed to the unabsorbed PT2385 fraction. The circulating drug-related metabolites are mainly composed of the unmodified PT2385, and to a much lesser extent, M1 and M8. Thus, it's less likely that M1 and M8 contribute to the pharmacological and toxicological effects of PT2385. Results from HLM and MLM experiments suggests that the mouse is a reasonable surrogate for predicting metabolism of this drug in humans. It should be noted that only male mice were used in the current study, because all the published preclinical studies for PT2385 and its analog PT2399 were done with males (Cho et al., 2016; Wallace et al., 2016).

Another important task in preclinical drug metabolism studies is phenotyping the enzymes involved in PT2385 metabolism, which facilitates the understanding of individual's response and could predict drug-drug interactions. The *in vitro* incubations of PT2385 with recombinant human phase I metabolizing enzymes reveal that multiple enzymes, including CYP2C19, CYP1A1, CYP1A2, CYP2D6, CYP2C9 and CYP3A4, participate in the hydroxylation metabolism of PT2385.

Among these enzymes, CYP2C19 is the predominant CYP involved in PT2385 oxidation. CYP2C19 plays a critical role in the metabolism of drugs, including anticancer, antidepressant, antihypertensive, antiplatelet and antiulcer drugs (Hirota et al., 2013). However, CYP2C19 is polymorphic with 12-23% of null alleles in Asians and 3-5% in Caucasians leading to significant inter-individual differences in activity that could result in different metabolism rates and fluctuations in exposure levels of PT2385 (Goldstein and de Morais, 1994; Umamaheswaran et al., 2014). For phase II metabolism, UGT1A family glucuronidates phenol metabolites (M1, M2, and M7), with UGT1A1/3 responsible for M10 and M12 formation, and UGT1A1/3/9 for M11 formation. UGT1A catalyzes the glucuronidation of a wide range of substrates, including endogenous substrates such as bilirubin, bile acids and steroids, as well as drugs and environment pollutants (Rowland et al., 2013). Moreover, UGT2B17 dominates the direct glucuronide conjugation of the aliphatic hydroxyl group in PT2385 to M8. UGT2B17 is mainly expressed in the liver with very low expression in the small intestine and kidney (Nakamura et al., 2008). M8 is the most abundant metabolite found in bile, which is formed in liver and quickly excreted in bile. It was also reported that UGT2B17 exhibited high expression in jejunum of morbidly obese subjects, and had the high inter-individual variation, which might be the result of genetic polymorphism (Miyauchi et al., 2016). Furthermore, the activity of UGT2B17 is also significantly impacted by complex factors, such as age, hormonal signaling, medications, supplements, alcohol consumption, and smoking (Neumann et al., 2016). Therefore, there might be significant inter-patient variability in drug metabolism in populations and drug-drug interactions of PT2385, and perhaps leading to increased toxicity or altered efficacy. Consistently, pharmacokinetic variability was observed in patients treated with PT2385 in the current phase I dose-escalation study (Courtney et al., 2017). To reduce the variability, PT2977 was developed with more potency, which is in a phase II trial in patients with advanced solid tumors.

DMD Fast Forward. Published on January 23, 2018 as DOI: 10.1124/dmd.117.079723
This article has not been copyedited and formatted. The final version may differ from this version.



Metabolomics analysis also reveals that PT2385 disrupted bile acid homeostasis, as shown by notably increased TCA and T-β-MCA in mice after PT2385 administration. TCA and T-β-MCA are major primary bile acids, constituting about 60% of the taurine-conjugated bile acids and 18% of total bile acids in mice (García-Cañaveras et al., 2012). The elevated TCA and T-β-MCA levels observed indicates that PT2385 may induce cholestasis after long-term application. It was reported that the ligand-activated nuclear receptors FXR mainly regulates bile acid synthesis enzymes and transporters by a complex network of transcriptional cascades (Eloranta and Kullak-Ublick, 2005). CYP7A1 catalyzes the first reaction in the cholesterol catabolic pathway in liver, and is the rate-limiting step in bile acid synthesis (Chiang, 2009). The expression of CYP7A1 is repressed by either SHP via liver FXR activation or FGF15 via intestine FXR activation (Goodwin et al., 2000; Inagaki et al., 2005). However, transcriptional analysis for bile acid synthesis genes reveals that among FXR and its target gene mRNAs in liver and intestine, only the expression of *Cyp7a1* mRNA in livers is upregulated by PT2385 treatment. Moreover, *Cyp7a1* mRNA levels are also increased in the livers of intestinal-specific *Hif2a* knockout mice. These data imply that PT2385 might upregulate liver CYP7A1 by inhibiting intestinal HIF-2α, independent of FXR signaling. Others reported that activation of hepatic HIF-2α leads to the inhibition of CYP7A1 by repressing the circadian expression of Rev-erbα, resulting in increased expression of E4BP4, a negative regulator of CYP7A1 (Ramakrishnan et al., 2014). However, neither PT2385 treatment nor intestinal *Hif2a* disruption affects hepatic HIF-2α signaling (Xie et al., 2017). The link between intestine HIF-2α and bile acid synthesis needs further investigation.

In conclusion, this study is the first report on PT2385 metabolism and its modulation of bile acid homeostasis. The metabolites from PT2385 are mainly derived from CYP2C19-mediated hydroxylation and oxidative defluorination, and UGT2B17 and UGT1A1/3-mediated

glucuronidation. The genetic polymorphisms of CYP2C19 and UGT2B17 may explain the individual variation observed during its clinical trial. Intestinal HIF-2α inhibition by PT2385 treatment disrupts bile acid homeostasis. The potential safety issues regarding long-term use of PT2385 need further assessment. Continued investigation into the connection between intestine HIF-2α and bile acid synthesis will be helpful in understanding the function of intestinal HIF-2α. Taken together, the information provided in the present study clarify the drug-organism interactions for PT2385, expand the substrate spectra for CYP2C19 and UGT2B17, and will be beneficial for further development of PT2385 or its structural analogues.

**Authorship Contributions.**

*Participated in research design:* Xie, Gao, Qin, Gonzalez.

*Conducted experiments:* Xie, Gao, Sun, Zhang, Krausz.

*Contributed new reagents or analytic tools:* Xie, Gao.

*Performed data analysis:* Xie, Gao.

*Wrote or contributed to the writing of the manuscript:* Xie, Gao, Gonzalez.

## References

Bertout JA, Majmundar AJ, Gordan JD, Lam JC, Ditsworth D, Keith B, Brown EJ, Nathanson KL, and Simon MC (2009) HIF2alpha inhibition promotes p53 pathway activity, tumor cell death, and radiation responses. *Proc Natl Acad Sci U S A* 106:14391-14396.

Chen W, Hill H, Christie A, Kim MS, Holloman E, Pavia-Jimenez A, Homayoun F, Ma Y, Patel N, Yell P, Hao G, Yousuf Q, Joyce A, Pedrosa I, Geiger H, Zhang H, Chang J, Gardner KH, Bruick RK, Reeves C, Hwang TH, Courtney K, Frenkel E, Sun X, Zojwalla N, Wong T, Rizzi JP, Wallace EM, Josey JA, Xie Y, Xie XJ, Kapur P, McKay RM, and Brugarolas J (2016) Targeting renal cell carcinoma with a HIF-2 antagonist. *Nature* **539:**112-117.

Chiang JY (2009) Bile acids: regulation of synthesis. *J Lipid Res* **50:**1955-1966.

Cho H, Du X, Rizzi JP, Liberzon E, Chakraborty AA, Gao W, Carvo I, Signoretti S, Bruick RK, Josey JA, Wallace EM, and Kaelin WG (2016) On-target efficacy of a HIF-2alpha antagonist in preclinical kidney cancer models. *Nature* **539:**107-111.

Courtney KD, Infante JR, Lam ET, Figlin RA, Rini BI, Brugarolas J, Zojwalla NJ, Lowe AM, Wang K, Wallace EM, Josey JA, and Choueiri TK (2017) Phase I Dose-Escalation Trial of PT2385, a First-in-Class Hypoxia-Inducible Factor-2alpha Antagonist in Patients With Previously Treated Advanced Clear Cell Renal Cell Carcinoma. *J Clin Oncol***:**JCO2017742627.

Eloranta JJ and Kullak-Ublick GA (2005) Coordinate transcriptional regulation of bile acid homeostasis and drug metabolism. *Archives of Biochemistry and Biophysics* **433:**397-412.

Epstein AC, Gleadle JM, McNeill LA, Hewitson KS, O'Rourke J, Mole DR, Mukherji M, Metzen E, Wilson MI, Dhanda A, Tian YM, Masson N, Hamilton DL, Jaakkola P, Barstead R, Hodgkin J, Maxwell PH, Pugh CW, Schofield CJ, and Ratcliffe PJ (2001) C. elegans EGL-9 and mammalian homologs define a family of dioxygenases that regulate HIF by prolyl hydroxylation. *Cell* **107:**43-54.

Fang ZZ and Gonzalez FJ (2014) LC-MS-based metabolomics: an update. *Arch Toxicol* **88:**1491-1502.

García-Cañaveras JC, Donato MT, Castell JV, and Lahoz A (2012) Targeted profiling of circulating and hepatic bile acids in human, mouse, and rat using a UPLC-MRM-MS-validated method. *Journal of lipid research* **53:**2231-2241.

Gnarra JR, Tory K, Weng Y, Schmidt L, Wei MH, Li H, Latif F, Liu S, Chen F, Duh FM, and et al. (1994) Mutations of the VHL tumour suppressor gene in renal carcinoma. *Nat Genet* **7:**85-90.

Goodwin B, Jones SA, Price RR, Watson MA, McKee DD, Moore LB, Galardi C, Wilson JG, Lewis MC, Roth ME, Maloney PR, Willson TM, and Kliewer SA (2000) A regulatory cascade of the nuclear receptors FXR, SHP-1, and LRH-1 represses bile acid biosynthesis. *Mol Cell* **6:**517-526.

Gordan JD, Bertout JA, Hu CJ, Diehl JA, and Simon MC (2007) HIF-2alpha promotes hypoxic cell proliferation by enhancing c-myc transcriptional activity. *Cancer Cell* **11:**335-347.

Hirota T, Eguchi S, and Ieiri I (2013) Impact of genetic polymorphisms in CYP2C9 and CYP2C19 on the pharmacokinetics of clinically used drugs. *Drug Metab Pharmacokinet* **28:**28-37.

Inagaki T, Choi M, Moschetta A, Peng L, Cummins CL, McDonald JG, Luo G, Jones SA, Goodwin B, and Richardson JA (2005) Fibroblast growth factor 15 functions as an enterohepatic signal to regulate bile acid homeostasis. *Cell metabolism* **2:**217-225.

Keith B, Johnson RS, and Simon MC (2012) HIF1α and HIF2α: sibling rivalry in hypoxic tumour growth and progression. *Nature Reviews Cancer* **12:**9-22.

Kondo K, Klco J, Nakamura E, Lechpammer M, and Kaelin WG (2002) Inhibition of HIF is necessary for tumor suppression by the von Hippel-Lindau protein. *Cancer cell* **1:**237-246.

Li T and Chiang JY (2015) Bile acids as metabolic regulators. *Current opinion in gastroenterology* **31:**159.

Matsubara T, Li F, and Gonzalez FJ (2013) FXR signaling in the enterohepatic system. *Mol Cell Endocrinol* **368:**17-29.

Maxwell PH, Wiesener MS, Chang GW, Clifford SC, Vaux EC, Cockman ME, Wykoff CC, Pugh CW, Maher ER, and Ratcliffe PJ (1999) The tumour suppressor protein VHL targets hypoxia-inducible factors for oxygen-dependent proteolysis. *Nature* **399:**271-275.

Meijer J, Bergstrand A, and DePierre JW (1987) Preparation and characterization of subcellular fractions from the liver of C57B1/6 mice, with special emphasis on their suitability for use in studies of epoxide hydrolase activities. *Biochem Pharmacol* **36:**1139-1151.

Miyauchi E, Tachikawa M, Decleves X, Uchida Y, Bouillot JL, Poitou C, Oppert JM, Mouly S, Bergmann JF, Terasaki T, Scherrmann JM, and Lloret-Linares C (2016) Quantitative Atlas of Cytochrome P450, UDP-Glucuronosyltransferase, and Transporter Proteins in Jejunum of Morbidly Obese Subjects. *Mol Pharm* **13:**2631-2640.

Muglia VF and Prando A (2015) Renal cell carcinoma: histological classification and correlation with imaging findings. *Radiol Bras* **48:**166-174.

Nakamura A, Nakajima M, Yamanaka H, Fujiwara R, and Yokoi T (2008) Expression of UGT1A and UGT2B mRNA in human normal tissues and various cell lines. *Drug Metabolism and Disposition* **36:**1461-1464.

Neumann E, Mehboob H, Ramirez J, Mirkov S, Zhang M, and Liu W (2016) Age-Dependent Hepatic UDP-Glucuronosyltransferase Gene Expression and Activity in Children. *Front Pharmacol* **7:**437.

Ramakrishnan SK, Taylor M, Qu A, Ahn S-H, Suresh MV, Raghavendran K, Gonzalez FJ, and Shah YM (2014) Loss of von Hippel-Lindau Protein (VHL) Increases Systemic Cholesterol Levels through Targeting Hypoxia-Inducible Factor 2α and Regulation of Bile Acid Homeostasis. *Mol Cell Biol* **34:**1208-1220.

Rowland A, Miners JO, and Mackenzie PI (2013) The UDP-glucuronosyltransferases: their role in drug metabolism and detoxification. *The international journal of biochemistry & cell biology* **45:**1121-1132.

Sato Y, Yoshizato T, Shiraishi Y, Maekawa S, Okuno Y, Kamura T, Shimamura T, Sato-Otsubo A, Nagae G, Suzuki H, Nagata Y, Yoshida K, Kon A, Suzuki Y, Chiba K, Tanaka H, Niida A, Fujimoto A, Tsunoda T, Morikawa T, Maeda D, Kume H, Sugano S, Fukayama M, Aburatani H, Sanada M, Miyano S, Homma Y, and Ogawa S (2013) Integrated molecular analysis of clear-cell renal cell carcinoma. *Nat Genet* **45:**860-867.

Semenza GL and Wang GL (1992) A nuclear factor induced by hypoxia via de novo protein synthesis binds to the human erythropoietin gene enhancer at a site required for transcriptional activation. *Mol Cell Biol* **12:**5447-5454.

Siegel RL, Miller KD, and Jemal A (2017) Cancer Statistics, 2017. *CA Cancer J Clin* **67:**7-30.

Vanharanta S, Shu W, Brenet F, Hakimi AA, Heguy A, Viale A, Reuter VE, Hsieh JJ, Scandura JM, and Massague J (2013) Epigenetic expansion of VHL-HIF signal output drives multiorgan metastasis in renal cancer. *Nat Med* **19:**50-56.

Wallace EM, Rizzi JP, Han G, Wehn PM, Cao Z, Du X, Cheng T, Czerwinski RM, Dixon DD, and Goggin BS (2016) A small-molecule antagonist of HIF2α is efficacious in preclinical models of renal cell carcinoma. *Cancer research* **76:**5491-5500.

Wishart DS (2016) Emerging applications of metabolomics in drug discovery and precision medicine. *Nat Rev Drug Discov* **15:**473-484.

Xie C, Yagai T, Luo Y, Liang X, Chen T, Wang Q, Sun D, Zhao J, Ramakrishnan SK, Sun L, Jiang C, Xue X, Tian Y, Krausz KW, Patterson AD, Shah YM, Wu Y, Jiang C, and Gonzalez FJ (2017) Activation of intestinal hypoxia-inducible factor 2alpha during obesity contributes to hepatic steatosis. *Nat Med*.

Xie C, Zhong D, Yu K, and Chen X (2012) Recent advances in metabolite identification and quantitative bioanalysis by LC-Q-TOF MS. *Bioanalysis* **4:**937-959.

Xie C, Zhou J, Guo Z, Diao X, Gao Z, Zhong D, Jiang H, Zhang L, and Chen X (2013) Metabolism and bioactivation of famitinib, a novel inhibitor of receptor tyrosine kinase, in cancer patients. *Br J Pharmacol* **168:**1687-1706.

**Footnotes**

This study was supported by the Intramural Research Program of the National Institutes of Health (National Cancer Institute) and the National Natural Science Foundation of China [Grant No. 81473415 and 81403007]. X.G. was supported by Shanxi University.

C.X. and X.G. are co-first authors.

Current affiliation for Dongxue Sun: College of Traditional Chinese Medicine, Shenyang Pharmaceutical University, Shenyang, Liaoning, 110016, China

Current affiliation for Youbo Zhang: State Key Laboratory of Natural and Biomimetic Drugs (Peking University) and Department of Natural Medicines, School of Pharmaceutical Sciences, Peking University, Beijing, 100191, China

DMD Fast Forward. Published on January 23, 2018 as DOI: 10.1124/dmd.117.079723
This article has not been copyedited and formatted. The final version may differ from this version.



**Legends for Figures**

**Fig. 1. Chromatography and mass spectra of PT2385 by UPLC-HRMS analysis.** (A) Chromatographic graph of PT2385; (B) MS spectrum of PT2385 in negative mode. (C) MS/MS spectrum of PT2385 in negative mode. (D) Tentative MS/MS fragmentation pattern of PT2385.

**Fig. 2. Multivariate data analysis and PT2385 metabolite identification.** Samples were collected from mice 24 h after orally administered with vehicle or PT2385 at a single dose of 50 mg/kg. (A, B) PCA score plot (A) and S-plot (B) of feces metabolome. (C, D) PCA score plot (C) and S-plot (D) of urine metabolome. (E, F) PCA score plot (E) and S-plot (F) of bile metabolome. (G, H) PCA score plot (G) and S-plot (H) of 3-h serum metabolome. Vehicle (■) and PT2385 (●). Each point represents an individual mouse sample in PCA score plot and a unique ion in S-plot.

**Fig. 3. MS/MS spectra and proposed fragmentation patterns of representative metabolites.** (A) M1. (B) M2. (C) M3 and M4. (D) M5 and M6. (E) M7. (F) M9. (G) M10. (H) M11.

**Fig. 4. Proposed metabolic pathways of PT2385 in mice.** Biotransformation pathways included hydroxylation (M1, M2), di-hydroxylation and desaturation (M3, M4), oxidative-defluorination (M7), glucuronidation (M8), *N*-acetylcysteine conjugation (M9), and secondary methylation (M5, M6) and glucuronidation (M10, M11, and M12).

**Fig. 5. *In vitro* metabolism of PT2385.** (A) PT2385 metabolism in HLM. (B) PT2385 metabolism in MLM. (C-E) The CYPs involved in M1 (C), M2 (D), and M7 (E) formation. (F-I) The UGTs involved in M8 (F), M10 (G), M11 (H) and M12 (I) formation.

**Fig. 6. Multivariate data analysis and endogenic metabolic profiling of PT2385.** Samples were collected from mice 24 h after orally administered with vehicle or PT2385 at a single dose of 50 mg/kg. (A, B) PCA score plot (A) and S-plot (B) of 24-h serum metabolome. (C, D) PCA score plot (C) and S-plot (D) of liver metabolome. Vehicle (■) and PT2385 (●). Each point represents an individual mouse sample in PCA score plot and a unique ion in S-plot. (E, F) Relative abundance of TCA and T-β-MCA in 24-h serum (E) and liver (F). Data are presented as mean ± s.e.m. $*P < 0.05$, or $**P < 0.01$, versus vehicle group, by two-tailed Student's t-test.

**Fig. 7. PT2385 treatment upregulates bile acid synthesis.** (A) Bile acid synthesis mRNAs in the livers after PT2385 exposure. (B) FXR and its target gene mRNAs in mouse liver after PT2385 exposure. (C) FXR and its target gene mRNAs in mouse intestine after PT2385 exposure. (D) Bile acid synthesis mRNAs in the livers of *Hif2a*$^{fl/fl}$ and *Hif2a*$^{\Delta IE}$ mice. Data are presented as mean ± s.e.m. $*P < 0.05$, or $**P < 0.01$, versus vehicle group or *Hif2a*$^{fl/fl}$ mice, by two-tailed Student's t-test.

**Table 1.** UPLC-HRMS data for PT2385 metabolites detected in mouse feces, urine, bile and serum

| No. | Metabolic pathway | *R*t (min) | Measured | Ion | Formula | Error (ppm) | Matrices* |
|---|---|---|---|---|---|---|---|
| M0 | Parent | 6.0 | 362.0309 | $[M-H-HF]^-$ | $C_{17}H_{12}F_3NO_4S$ | 2.8 | F, U, S, B |
| M1 | Hydroxylation | 5.5 | 398.0313 | $[M-H]^-$ | $C_{17}H_{12}F_3NO_5S$ | 0.8 | F, U, S, B |
| M2 | Hydroxylation | 5.7 | 398.0303 | $[M-H]^-$ | $C_{17}H_{12}F_3NO_5S$ | -1.8 | F, U, B |
| M3 | 2 × Hydroxylation + Desaturation | 5.3 | 412.0156 | $[M-H]^-$ | $C_{17}H_{10}F_3NO_6S$ | 14.0 | F |
| M4 | 2 × Hydroxylation + Desaturation | 5.4 | 412.0123 | $[M-H]^-$ | $C_{17}H_{10}F_3NO_6S$ | 4.9 | F |
| M5 | 2 × Hydroxylation + Desaturation + Methylation | 5.8 | 426.0297 | $[M-H]^-$ | $C_{18}H_{12}F_3NO_6S$ | 8.8 | F |
| M6 | 2 × Hydroxylation + Desaturation + Methylation | 5.9 | 426.0289 | $[M-H]^-$ | $C_{18}H_{12}F_3NO_6S$ | 7.0 | F, U |
| M7 | Oxidative Defluorination | 5.6 | 380.0421 | $[M-H]^-$ | $C_{17}H_{13}F_2NO_5S$ | 4.5 | F, B |
| M8 | Glucuronide conjugation | 5.5 | 558.0701 | $[M-H]^-$ | $C_{23}H_{20}F_3NO_{10}S$ | 3.4 | U, B, S |
| M9 | N-acetylcysteine conjugation | 5.8 | 543.0534 | $[M-H]^-$ | $C_{22}H_{19}F_3N_2O_7S_2$ | 4.8 | U |
| M10 | Hydroxylation + glucuronide conjugation | 4.8 | 574.0661 | $[M-H]^-$ | $C_{23}H_{20}F_3NO_{11}S$ | 5.2 | U, B |
| M11 | Hydroxylation + glucuronide conjugation | 5.1 | 574.0661 | $[M-H]^-$ | $C_{23}H_{20}F_3NO_{11}S$ | 5.2 | U |
| M12 | Oxidative Defluorination+ glucuronide conjugation | 5.0 | 557.0758 | $[M-H]^-$ | $C_{23}H_{21}F_2NO_{11}S$ | 5.9 | B |

***** F, Feces; U, Urine; S, Serum; B, Bile.

DMD Fast Forward. Published on January 23, 2018 as DOI: 10.1124/dmd.117.079723
This article has not been copyedited and formatted. The final version may differ from this version.



## Figure 1

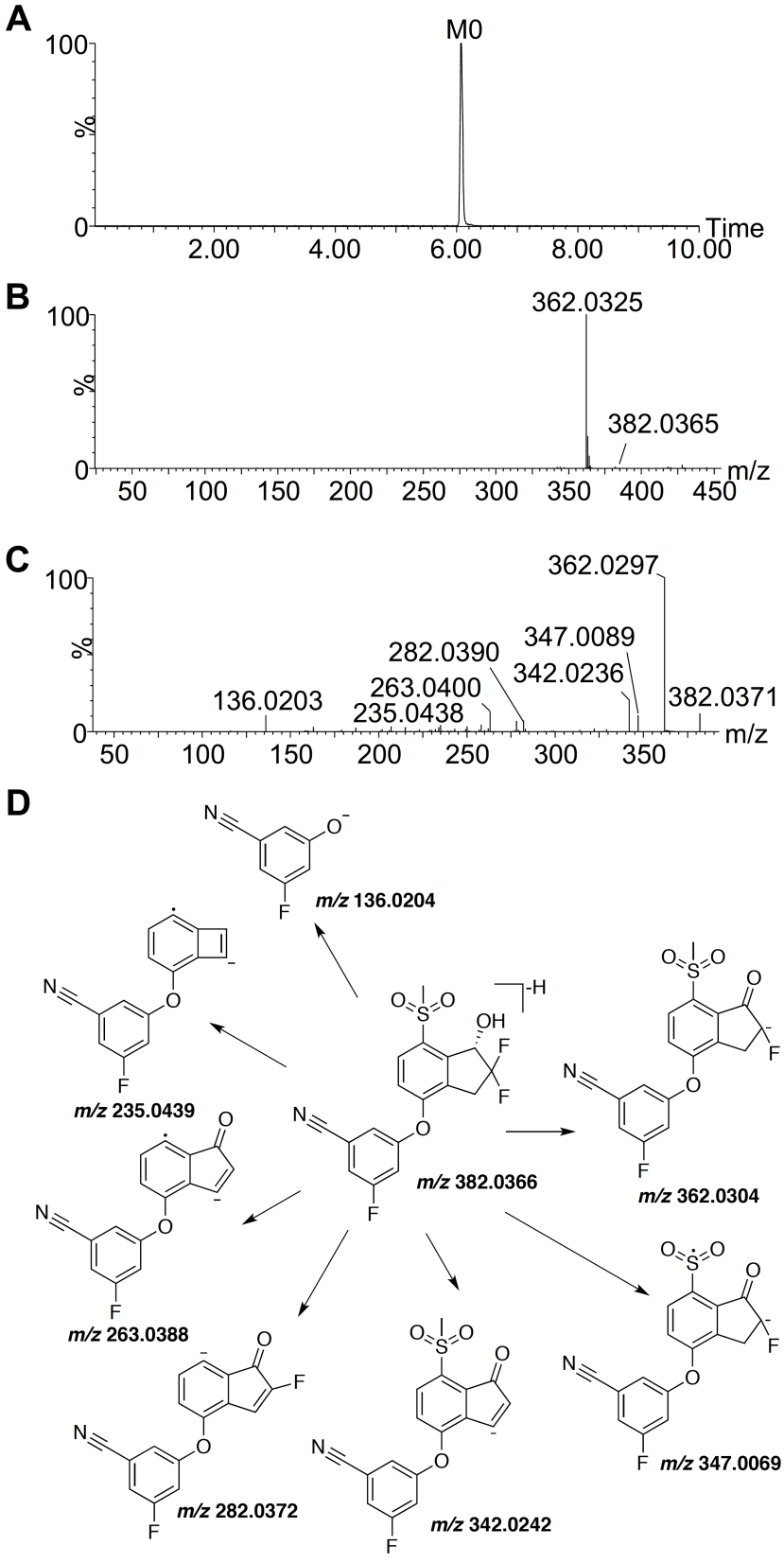

DMD Fast Forward. Published on January 23, 2018 as DOI: 10.1124/dmd.117.079723
This article has not been copyedited and formatted. The final version may differ from this version.



## Figure 2

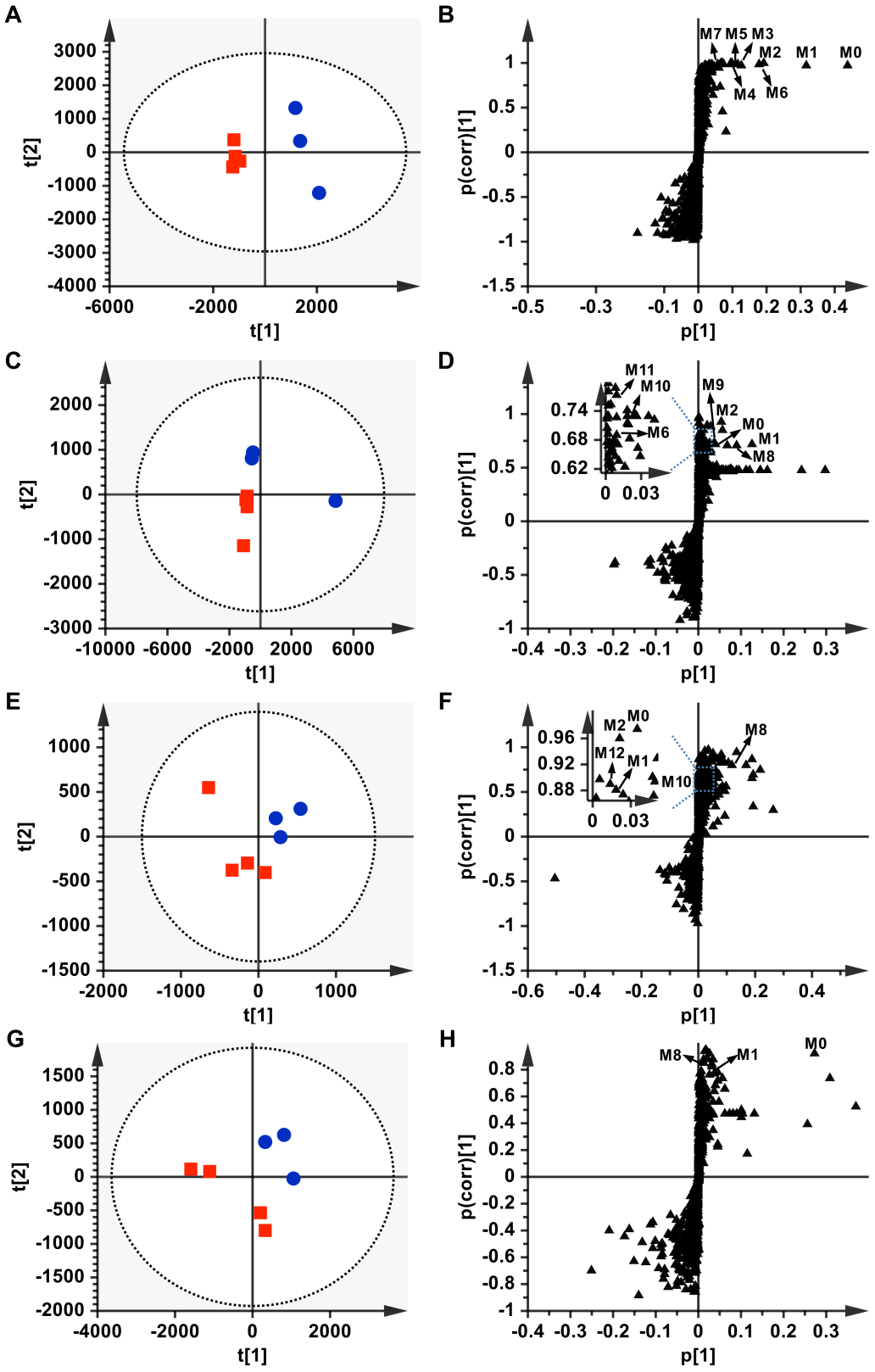

DMD Fast Forward. Published on January 23, 2018 as DOI: 10.1124/dmd.117.079723
This article has not been copyedited and formatted. The final version may differ from this version.



# Figure 3

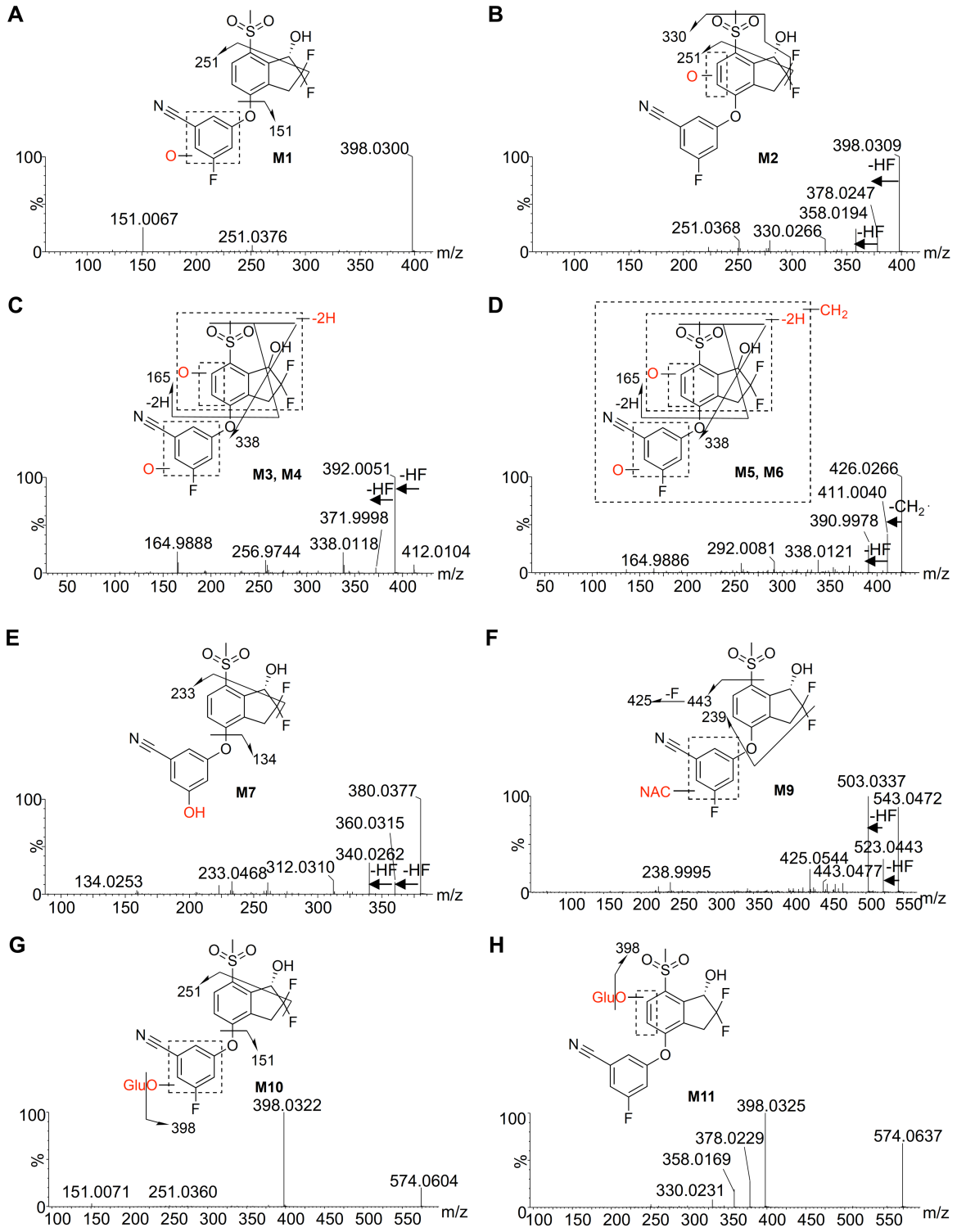

DMD Fast Forward. Published on January 23, 2018 as DOI: 10.1124/dmd.117.079723
This article has not been copyedited and formatted. The final version may differ from this version.



# Figure 4

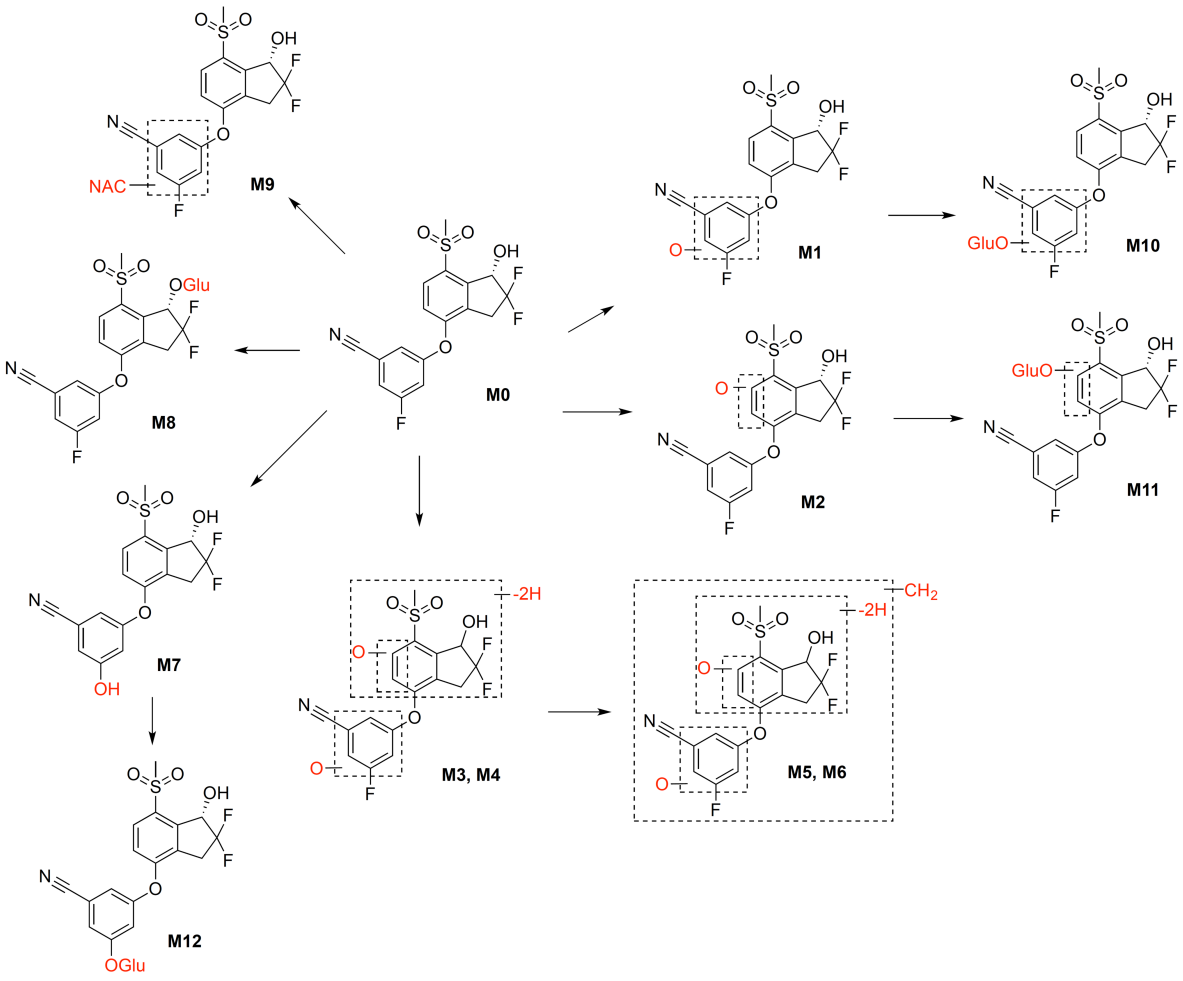

DMD Fast Forward. Published on January 23, 2018 as DOI: 10.1124/dmd.117.079723
This article has not been copyedited and formatted. The final version may differ from this version.



# Figure 5

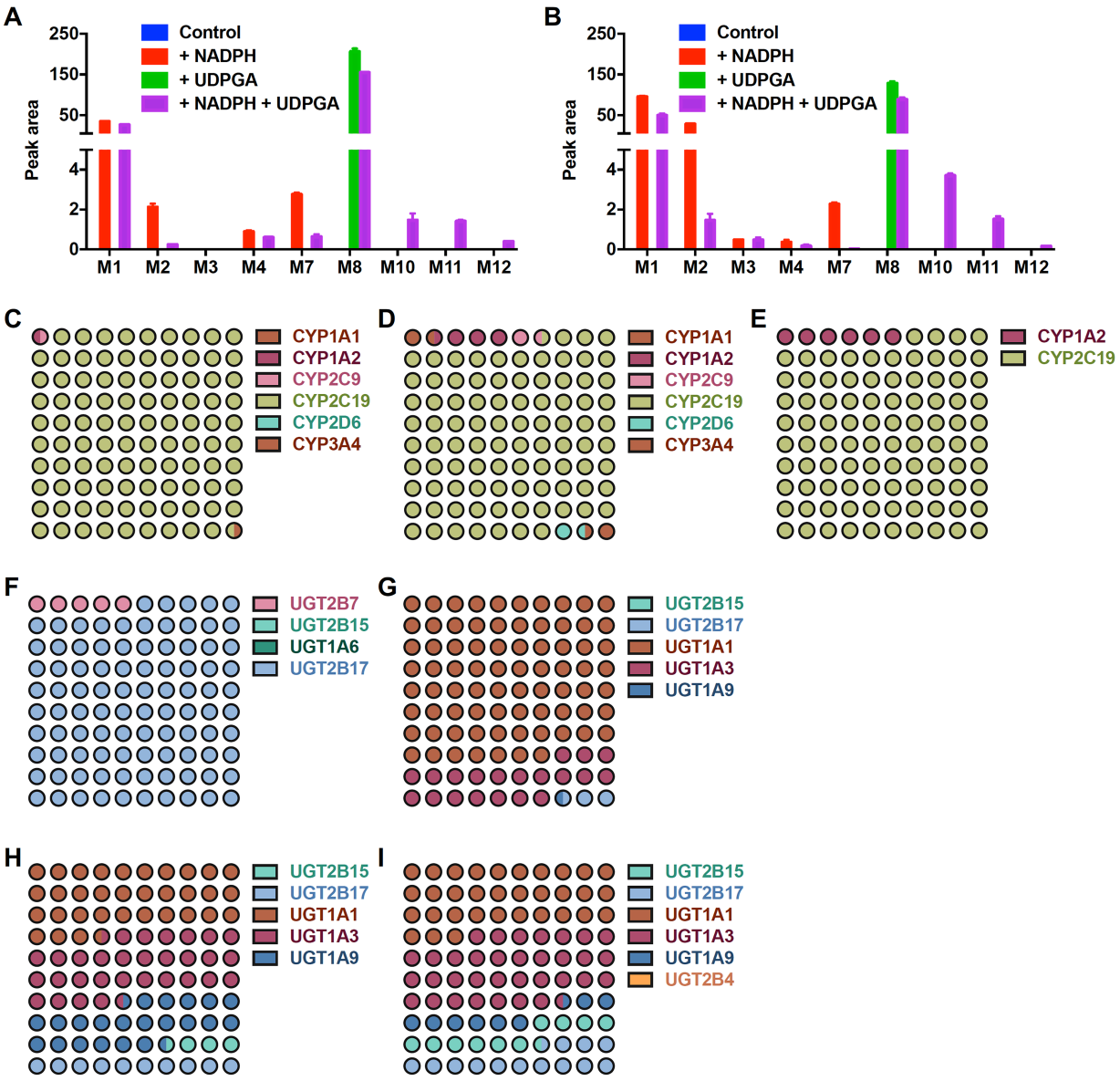

DMD Fast Forward. Published on January 23, 2018 as DOI: 10.1124/dmd.117.079723
This article has not been copyedited and formatted. The final version may differ from this version.



# Figure 6

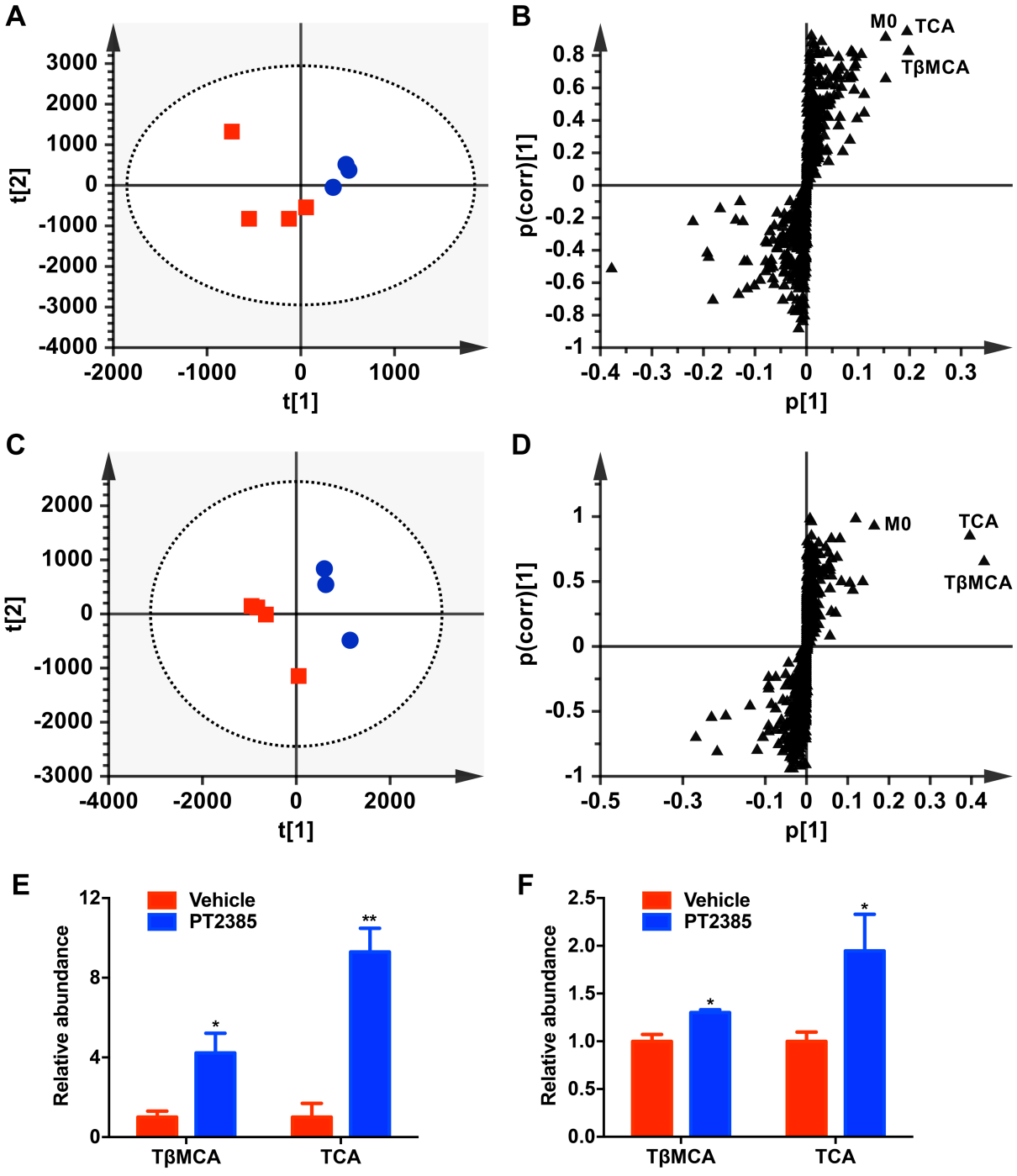

DMD Fast Forward. Published on January 23, 2018 as DOI: 10.1124/dmd.117.079723
This article has not been copyedited and formatted. The final version may differ from this version.



# Figure 7